

# THYME: Temporal Hierarchical-Cyclic Interactivity Modeling for Video Scene Graphs in Aerial Footage

Trong-Thuan Nguyen, *Member, IEEE*, Pha Nguyen, *Member, IEEE*, Jackson Cothren, *Member, IEEE*, Alper Yilmaz, *Senior Member, IEEE*, Minh-Triet Tran, *Member, IEEE*, and Khoa Luu, *Senior Member, IEEE*

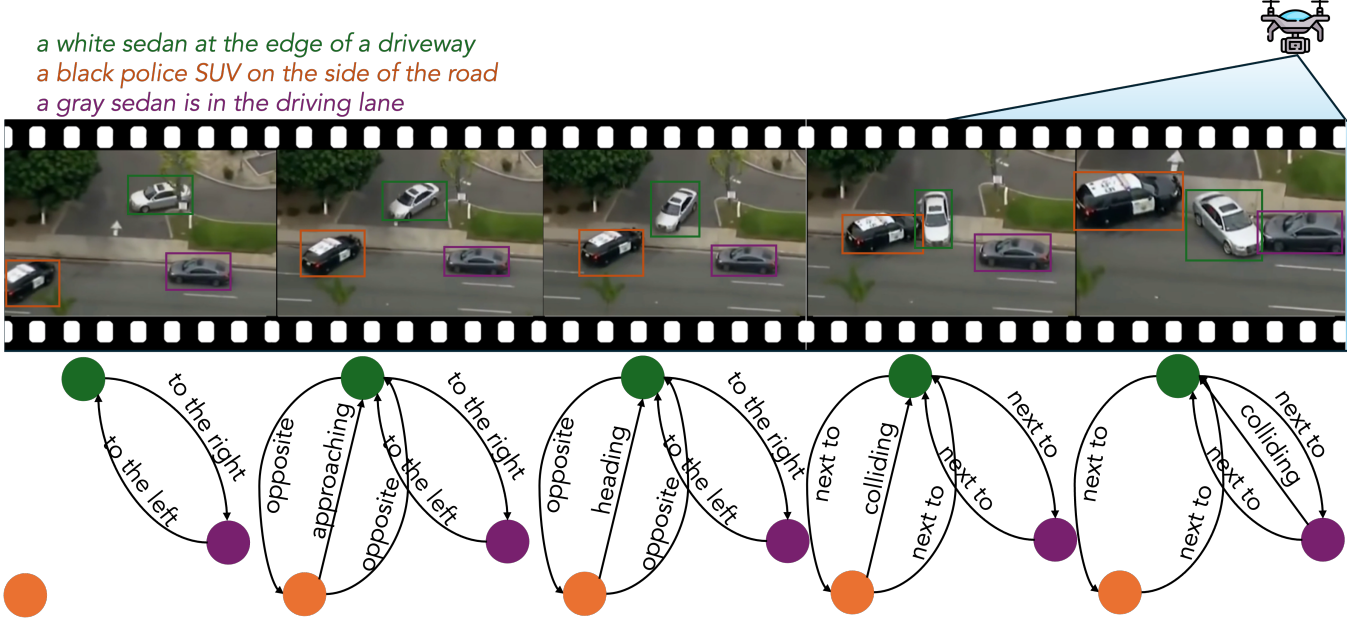


Fig. 1: An exemplar video from the proposed **AeroEye-v1.0** dataset, captured by a drone, is annotated with *five interactivity types*: appearance, situation, position, interaction, and relation. Specifically, the proposed **THYME** approach then generates frame-by-frame scene graphs, hierarchically aggregating per-frame object features and refining them through cyclic temporal attention. Therefore, our proposed **THYME** approach accurately tracks the white sedan turning out, the police SUV converging, and the gray sedan being impacted, effectively capturing subtle transitions in interactivity. (**Best viewed in colors**)

**Abstract**—The rapid proliferation of video in applications such as autonomous driving, surveillance, and sports analytics necessitates robust methods for dynamic scene understanding. Despite advances in static scene graph generation and early attempts at video scene graph generation, previous methods often suffer from fragmented representations, failing to capture fine-grained spatial details and long-range temporal dependencies simultaneously. To address these limitations, we introduce the Temporal Hierarchical Cyclic Scene Graph (THYME) approach, which synergistically integrates hierarchical feature aggregation with cyclic temporal refinement to address these limitations. In particular, THYME effectively models multi-scale spatial context and enforces temporal consistency across frames, yielding more accurate and coherent scene graphs. In addition, we present AeroEye-v1.0, a novel aerial video dataset enriched with five types of interactivity that overcome the constraints of existing datasets and provide a comprehensive benchmark for dynamic scene graph generation. Empirically, extensive experiments on ASPIRE and AeroEye-v1.0 demonstrate that the proposed THYME approach outperforms state-of-the-art methods, offering improved scene understanding in ground-view and aerial scenarios.

**Index Terms**—Video Scene Graph Generation, Video Understanding, Hierarchical Graph, Graph Transformer, Aerial Footage

Trong-Thuan Nguyen is with University of Arkansas; University of Science, VNU-HCM; Vietnam National University, Ho Chi Minh, Viet Nam. Pha Nguyen, Jackson Cothren, Khoa Luu are with University of Arkansas. Alper Yilmaz is with Ohio State University. Minh-Triet Tran is with University of Science, VNU-HCM; Vietnam National University, Ho Chi Minh, Viet Nam.

## I. INTRODUCTION

The proliferation of video data across various domains, including autonomous driving, aerial surveillance, robotics, sports analytics, and urban monitoring, has increased the need for methods to generate semantically rich and temporally coherent representations of dynamic scenes. Video Scene Graph Generation (VidSGG) addresses this challenge by constructing spatio-temporal graphs where nodes correspond to object trajectories and edges encode both spatial relations (e.g., in front of, adjacent to) and transient interactions (e.g., approaching, heading, overtaking, colliding). Although substantial progress has been made in image-based Scene Graph Generation (SGG), primarily driven by large-scale datasets such as Visual Genome [24], VG-150 [49], and OpenPSG [51], extending these techniques to the video domain presents considerable challenges. One of them is addressing temporal inconsistencies resulting from variations in appearance, occlusions, and the re-entry of objects. These factors can undermine the continuity and integrity of object identities over time. Additionally, the multi-scale nature of real-world video content requires hierarchical reasoning mechanisms that can capture fine-grained spatial details while maintaining coherent global structures over time.

Recent developments in VidSGG continue to exhibit notable limitations in capturing the full complexity of dynamic scenes. Although effective in extracting fine-grained spatial information,

frame-level methods [27], [5], [16], [12] often result in inconsistent relational predictions over time, particularly in the form of predicate flickering, and struggle to detect brief or subtle interactions. In contrast, video-level methods [41], [9], [25], [13], [44] that integrate temporal context tend to overlook fleeting relational dynamics and dilute the precision of spatial configurations, especially under aerial or oblique viewpoints where object scale and orientation vary significantly. Even the most state-of-the-art models [52], [32], [33] offer only partial improvements, frequently underrepresenting micro-interactions and nuanced spatial semantics. These observations underscore the need for a new approach to jointly model temporally coherent trajectories and preserve the structural richness of spatial relations in complex visual environments.

A significant challenge in Video Scene Graph Generation is balancing detailed spatial representations for each frame and consistent relational transitions over time. Although frame-centric pipelines are adept at capturing intricate geometric details, they often fail to produce cohesive and unified scene graphs, especially when objects are in motion, obscured, or reintroduced to the scene. In contrast, models that strive for temporal consistency typically rely on aggregation over extended periods, which can limit their responsiveness to brief yet critical interactions. Moreover, current benchmarks, most notably Action Genome [17], ASPIRe [32] and AeroEye [33], pose additional hurdles to advancement. Specifically, they offer narrow predicate vocabularies and lack sufficient viewpoint diversity, significantly impeding the adaptability of current methods to the rich and complex scenarios in video data.

To address these gaps, we propose the new *Temporal Hierarchical Cyclic Interactivity Model for Video Scene Graphs (THYME)* approach, which first performs multi-scale intra-frame aggregation to preserve local structure and then applies cyclic temporal attention to ensure long-range coherence. In addition, we introduce AeroEye-v1.0, a new aerial video data set annotated with five distinct interactivity types ( *i.e.* *appearance*, *situation*, *position*, *interaction*, and *relation*), providing the detailed, viewpoint-diverse supervision necessary for fine-grained and temporally aware scene understanding.

The contributions of this work can be summarized as follows:

- We propose the *Temporal Hierarchical Cyclic Interactivity Model for Video Scene Graphs (THYME)* approach, a novel architecture that synergistically integrates hierarchical feature aggregation and cyclic temporal refinement. This design enables THYME to capture multi-scale spatial details and long-range temporal dependencies more effectively than previous methods, resulting in more comprehensive and balanced scene graph representations.
- In contrast to existing methods that struggle to capture fine-grained spatial details and long-range temporal dependencies, THYME effectively integrates hierarchical feature aggregation with cyclic temporal refinement. Therefore, it generates a more accurate and coherent scene graph by preserving spatial context across multiple scales while ensuring temporal consistency across video frames.
- We introduce AeroEye-v1.0, a new aerial video dataset with detailed annotations across five types of interactivity.

AeroEye-v1.0 is designed to tackle the unique challenges of dynamic scene graph generation in aerial environments.

- To the best of our knowledge, AeroEye-v1.0 is one of the first datasets that can represent the most significant and richly annotated aerial video benchmark for VidSGG, as compared in Table I. It provides comprehensive annotations across five types of interactivity ( *i.e.*, *appearance*, *situation*, *position*, *interaction*, and *relationship*), enabling fine-grained characterization of object behaviors and spatial dynamics. In addition, our AeroEye-v1.0 dataset includes footage captured from aerial, oblique, and ground perspectives, offering a diverse and challenging corpus for dynamic scene graphs in aerial environments.
- Experimental results demonstrate that THYME establishes a new state-of-the-art on the ASPIRe and AeroEye-v1.0 benchmarks, achieving consistent improvements of 2 to 3% in recall and mean recall over the baseline methods. These performance margins support the efficiency of THYME’s dynamic scene graph generation efficiency across wild ground-view footage and drone-captured aerial videos.

The remainder of this paper is organized as follows. Sec. II reviews related work in SGG and video understanding. Sec. IV presents the THYME approach. Sec. V introduces the AeroEye-v1.0 dataset and its annotation methodology. In Sec. VI, we present our experimental setup, results, and analyses. Finally, Sect. VII concludes our research and describes future directions.

## II. RELATED WORK

### A. Background

Hierarchical graph representations have emerged as a natural way to model the temporal and multi-scale nature of video data. In particular, low-level features extracted from raw pixels or early convolutional layers are first organized into fine-grained structures in these approaches, such as objects, regions, or atomic actions. These local entities are progressively aggregated into higher-level semantic nodes, constructing a contextual information pyramid. Specifically, this hierarchical structure enables models to capture short-term interactions, such as localized object relationships [34], [7], [20], and long-term dependencies [53], [2], [15], including scene transitions [58], [55] or action progressions [26], [40].

Transformer-based architectures have revolutionized sequential modeling and are increasingly applied to graphs. Specifically, graph transformers [54] extend the self-attention mechanism in conventional transformers to non-Euclidean data structures by allowing every node in a graph to dynamically attend to every other node. This capability is particularly beneficial in video understanding, where temporal evolution and spatial layout are deeply intertwined. In addition, graph transformers capture long-range dependencies while integrating structural biases and positional encodings that respect the underlying graph connectivity. By leveraging self-attention [43], these models compute adaptive weights for nodes and selectively aggregate relevant contextual information. Such mechanisms have proven crucial in tasks such as action recognition [30], [35], [8], video question answering [47], [48], [10], and trajectory prediction [29], [18], [50], where modeling complex interrelations over time dramatically improves performance.

TABLE I: Comparisons of scene graph generation datasets. The upper block lists image-based scene graph generation datasets, while the lower block presents video-based scene graph generation datasets. The symbol # indicates the number of corresponding items. The best values within each block are **highlighted**.

Datasets	#Videos	#Frames	#ObjCls	#RelCls	#Scenes	Interactivity Types					Viewpoints		
						Appearance	Situation	Position	Interaction	Relation	aerial	oblique	ground
<b>Visual Genome</b> [24]	-	<b>108K</b>	<b>33K</b>	<b>42K</b>	-	×	×	×	✓	✓	×	×	✓
<b>VG-150</b> [49]	-	88K	150	50	-	×	×	×	✓	✓	×	×	✓
<b>VrR-VG</b> [28]	-	59K	1.6K	117	-	×	×	×	✓	✓	×	×	✓
<b>GQA</b> [14]	-	85K	1.7K	310	-	×	×	×	✓	✓	×	×	✓
<b>PSG</b> [51]	-	49K	80	56	-	×	×	×	✓	✓	×	×	✓
<b>VidOR</b> [37]	<b>10K</b>	55.4K	80	50	1	×	×	×	✓	✓	×	×	✓
<b>Action Genome</b> [17]	<b>10K</b>	234.3K	25	25	-	×	×	×	✓	✓	×	×	✓
<b>VidSTG</b> [56]	<b>10K</b>	55.4K	80	50	1	×	×	×	✓	✓	×	×	✓
<b>EPIC-KITCHENS</b> [6]	700	11.5K	21	13	1	×	×	×	✓	✓	×	×	✓
<b>PVSG</b> [52]	400	153K	126	57	7	×	×	×	✓	✓	×	✓	×
<b>SportsHHI</b> [46]	80	11.4K	1	34	2	×	×	×	✓	×	×	×	✓
<b>ASPIRe</b> [32]	1.5K	1.6M	<b>833</b>	<b>4.5K</b>	7	✓	✓	✓	✓	✓	×	×	✓
<b>AeroEye</b> [33]	2.3K	<b>261.5K</b>	57	384	<b>29</b>	×	×	✓	×	×	✓	✓	✓
<b>AeroEye-v1.0 (Ours)</b>	2.3K	<b>261.5K</b>	57	687	<b>29</b>	✓	✓	✓	✓	✓	✓	✓	✓

### B. Datasets and Benchmarks

**Datasets.** SGG has traditionally centered on *image-based* datasets, most notably *Visual Genome* [24]. *Visual Genome* provides a comprehensive collection of static images annotated with objects and their relationships. Its comprehensiveness has established it as a primary benchmark for SGG, despite being restricted to 3rd-person imagery. The following works have refined or extended Visual Genome’s foundational dataset. For example, *VG-150* [49] curates a more tractable subset, *VrR-VG* [28] enriches spatial relationships, and *GQA* [14] aligns the structure of the scene graph with reasoning tasks. Specifically, *PSG* [51] integrates panoptic segmentation with scene graphs, providing a holistic visual representation of the scene.

Recognizing the importance of *temporal dynamics*, VidSGG datasets have emerged to capture *transformations of relationships between frames*. *VidVRD* [39] provides an early benchmark dataset featuring 1K videos annotated with bounding boxes and spatiotemporal relations. This strategy is subsequently scaled by *VidOR* [37] and *Action Genome* [17], each comprising 10K videos with extensive annotations (e.g., 50K instances for VidOR and 476.3K for Action Genome). Similarly, *VidSTG* [56] is based on grounding interactions within video data, while *EPIC-KITCHENS* [6] provides extensive footage of kitchen activities. Building on *PSG* [51], *PVSG* [52] integrates panoptic segmentation to improve scene representation, while *SportsHHI* [46] focuses on capturing sports-related interactions.

In pursuit of *diverse perspectives*, *ASPIRe* [32] incorporates views of ego and 3rd-person views, facilitating multi-viewpoint and temporal modeling. Likewise, *AeroEye* [33] uniquely encompasses drone views, broadening the scope of SGG to aerial surveillance. Table I presents a comprehensive overview of these datasets, comparing their annotation scales, object and relation classes, and respective viewpoints.

**Benchmarks.** *Image Scene Graph Generation (ImgSGG)* focuses on detecting and classifying object relationships in static images, the primary challenge being the accurate categorization of these relationships according to a predefined set of predicates. Specifically, transformer-based methods [27], [12], [16], [45] and generative models [25], [22], [11] have significantly

advanced *ImgSGG* by leveraging attention mechanisms and generative frameworks to encode complex dependencies. Benchmark datasets such as *Visual Genome* [24], *VG-150* [49], *VrR-VG* [28], and *PSG* [51] offer large-scale annotations that drive model development. Thus, progress in *ImgSGG* has enabled models to capture nuanced relational semantics in static scenes.

Further enhancements have been achieved through bias reduction and the integration of external knowledge. Specifically, methods such as those proposed in *EOA* [3] and *C-SGG* [19] improve the recall of rare predicates and mitigate the biases inherent in SGG. In addition, segmentation and panoptic methods, exemplified by *Segmentation-SG* [21] and *PSGFormer* [51], enrich frame-level representations by incorporating pixel-level cues, producing more context-aware graphs. Moreover, open-vocabulary methods supported by vision-language models, which enable the recognition of unseen object classes and relationships, as well as the integration of LLMs as demonstrated in *LLM4SGG* [23] and text-based scene graph frameworks such as *TextPSG* [57].

*Video Scene Graph Generation (VidSGG)* extends *ImgSGG* by incorporating the temporal dimension, requiring models to capture evolving interactions across consecutive frames and aggregate spatiotemporal cues to construct coherent scene graphs. In particular, the methods utilize temporal modeling [36], [4] and further extend to hierarchical structures [41], [32] or transformer-based architectures [9], [31] that leverage self-attention to manage long-range dependencies. Benchmarks such as *Action Genome* [17], *PVSG* [52], *ASPIRe* [32], and *AeroEye* [33] offer diverse tasks reflecting the scope of spatiotemporal understanding, thereby substantiating the role of *VidSGG* in applications that demand robust temporal modeling.

### C. Video Scene Graph Generation

Current *VidSGG* methods are generally divided into two primary categories based on the granularity of their scene graph representation: *video-level SGG*, which captures persistent relationships across entire videos, and *frame-level SGG*, which focuses on dynamic interactions within individual frames.



**Video-level Scene Graph Generation.** Video-level SGG conceptualizes object trajectories as graph nodes to encapsulate stable and persistent relationships throughout a video. This approach leverages temporal continuity by modeling spatial and temporal statistical dependencies, thereby establishing relational associations. Early methodologies used techniques such as Conditional Random Fields (CRFs) [42], abstraction methods [36], and iterative relation inference on fully connected spatio-temporal graphs [38]. More recent advances have incorporated transformer-based frameworks to further enhance video performance. For example, unified frameworks that integrate scene graph generation with human-object interaction detection [13] and generative transformer approaches, such as IS-GGT [25], have been developed to efficiently capture persistent relationships across video frames.

Recently, video-level methods have increasingly emphasized explicit temporal modeling. PVSG [52] integrates panoptic segmentation masks with temporal scene graphs to ensure high-fidelity spatial detail and robust temporal coherence. Similarly, TRACE [41] effectively leverages spatio-temporal context, while methods like DSG-DETR [9] and OED [44] focus on modeling extended temporal relationships across object tracklets. These video-level SGG methods collectively underscore the efficacy of handling temporal consistency to construct scene graphs that comprehensively represent videos.

**Frame-level Scene Graph Generation.** Frame-level SGG constructs a scene graph for each frame, capturing dynamic interactions and providing a detailed description of scene dynamics as relationships transition between frames. Notably, transformer-based methods have been widely adopted because of their ability to infer relationships from features via attention mechanisms directly. For example, SGTR [27], ReITR [5], EGTR [16], and DSGG [12] employ encoder-decoder frameworks augmented with techniques such as bipartite graph matching, graph-aware query formulation, and relation distillation, thus achieving state-of-the-art performances while maintaining computational efficiency per frame basis.

Building on these transformer-based methods, CYCLO [33] introduces a cyclic attention mechanism to capture the periodic and overlapping relationships inherent in video. In contrast, HIG [32] employs hierarchical structures to model fine-grained and high-level interactivity patterns, thus improving the robustness of generated scene graphs. Moreover, recent work has addressed the issues of bias reduction and context augmentation at the frame level in SGG. Methods such as TEMPURA [31] and Fast C-SGG [19] integrate context augmentation, memory-guided training, and uncertainty attenuation to mitigate the adverse effects of biased annotations, ensuring that per-frame predictions remain robust even in complex scenes. Collectively, these methodologies, including transformer-based architectures, hierarchical modeling, and bias reduction techniques, have advanced frame-level SGG by enabling accurate and efficient per-frame scene graph generation and providing a robust foundation for temporal integration and dynamic scene analysis.

### III. PROBLEM ANALYSIS AND THE PROPOSED CONTRIBUTIONS

#### A. Prior Scene-Graph Modeling Methods and Their Limitations

Video-level SGG captures long-term relationships by tracking objects and modeling persistent interactions throughout a video. TRACE [41] and PVSG [52] establish stable relational structures, making them effective for long-term surveillance and human-object interaction tracking applications. For example, in traffic monitoring, these models can track vehicles across an intersection to determine right-of-way violations. However, these methods assume that the relationships remain stable over time, which is not always true in dynamic environments where interactions frequently change. A pedestrian may briefly interact with a cyclist before moving toward a different object, making static relationship tracking ineffective. These methods rely on object tracking, which can lead to error propagation. If a vehicle is lost due to occlusion, the entire relationship chain may break, leading to incorrect predictions.

In contrast, frame-level SGG constructs independent scene graphs for each frame, enabling fine-grained relational modeling. Transformer-based approaches such as SGTR [27], EGTR [16], and DSGG [12] effectively capture momentary object-object interactions. For example, in a sports analytics application, a frame-based model can detect a player passing a ball at a specific moment. However, since these models lack temporal coherence, they treat each frame as an isolated entity, leading to inconsistent relationship tracking across frames. If a model detects a pass in one frame but loses context in the next, it may fail to register the receiver's movement, resulting in fragmented tracking. These models also incur high computational costs, since they generate a scene graph at every frame. Without temporal memory mechanisms, they struggle to maintain contextual awareness, making them unreliable in fast-paced scenarios where relationships constantly shift.

To address the aforementioned limitations, HIG [32] (see Fig. 2a) introduces a hierarchical framework that merges single-frame interactivities into multi-frame interlacements, thereby constructing structured representations across multiple temporal scales. This approach effectively preserves both fine-grained interactions and higher-order relational patterns, enabling the maintenance of object relationships over extended temporal sequences. Unlike frame-based models, HIG integrates temporal dependencies by linking relational information across abstraction levels, thus offering a more holistic understanding of scene dynamics. A notable strength of HIG is its capacity to capture five distinct types of interactivity (i.e., appearance, situation, position, interaction, and relation), facilitating nuanced modeling of multi-object interactions. However, the framework lacks mechanisms for cyclic modeling, which limits its effectiveness in representing recurrent behaviors, such as vehicles stopping at traffic lights. Its dependence on fixed temporal segmentation further restricts adaptability to non-uniform interaction durations, such as the variable pacing of basketball plays. Moreover, while HIG demonstrates strong hierarchical aggregation capabilities, it does not explicitly enforce frame-to-frame consistency, which may result in representational errors in scenarios characterized by rapid shifts.



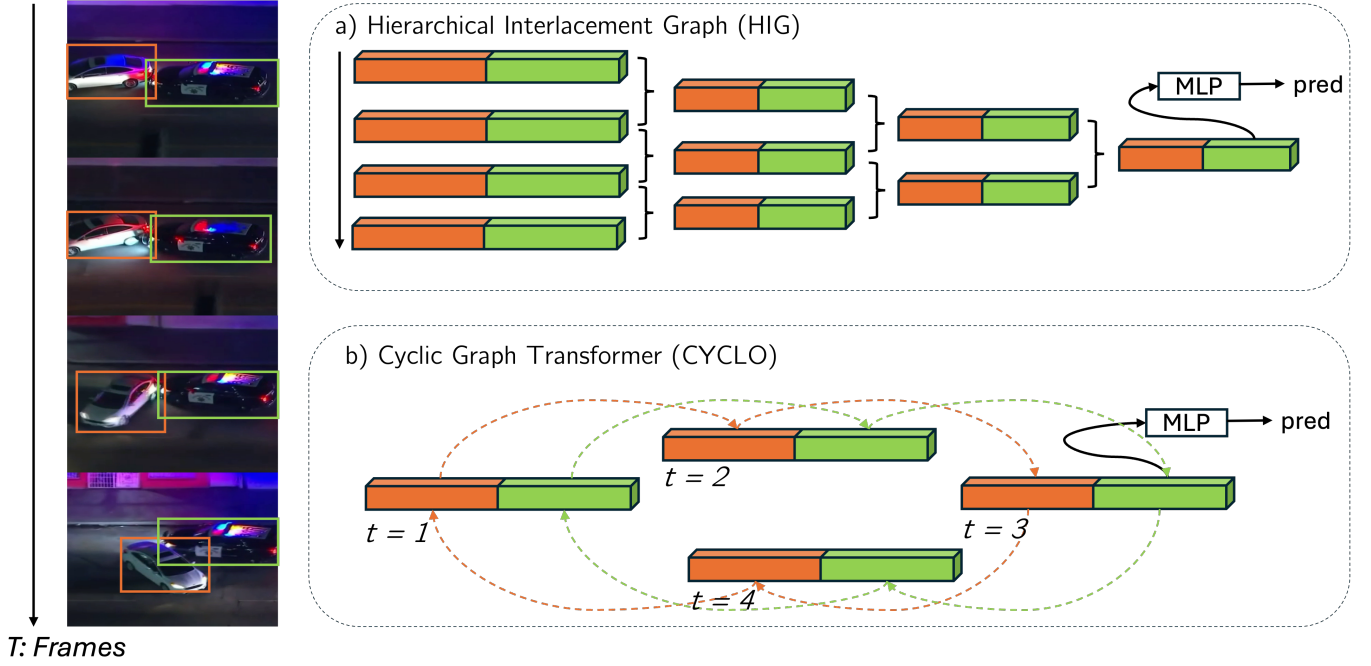


Fig. 2: (a) HIG [32] stacks single-frame progressively coarser layers; however, its fixed temporal windows and acyclic flow limit the modeling of recurrence and frame-to-frame coherence. (b) CYCLO [33] employs a ring-shaped spatio-temporal transformer whose cyclic attention links the clip’s tail back to its head, preserving long-range context and preventing relation drift, yet operates at a single spatial scale and omits explicit semantic axes. **(Best viewed in colors)**

CYCLO [33] (see Fig. 2b) introduces a cyclic spatio-temporal graph transformer that connects the end of a video sequence to its beginning, thereby preserving historical context and mitigating relational fragmentation in extended video streams. Its cyclic attention mechanism maintains temporal directionality, allowing relational dynamics to evolve sequentially rather than being treated as independent across frames. This design proves particularly effective in domains such as sports analytics, where continuity of action is critical; for example, in a tennis rally, CYCLO ensures that the ball’s trajectory remains temporally coherent across exchanges. Despite these strengths, CYCLO does not incorporate hierarchical structuring, which limits its ability to model multi-scale interactions in complex environments, such as crowd dynamics or group behaviors. Furthermore, CYCLO does not explicitly distinguish between different types of interactivity. Instead, it emphasizes spatial and temporal dependencies. As a result, it is less equipped to capture the semantic granularity necessary for scene understanding.

#### B. Our Proposed Approach and Its Advantages

One of the primary advantages of our THYME approach lies in integrating hierarchical feature aggregation with cyclic temporal refinement. As detailed in Sec. IV and demonstrated in recent work [32], hierarchical aggregation enables our model to fuse spatial features across multiple levels of abstraction progressively. This design effectively captures fine-grained details and global context, crucial for understanding cluttered or densely populated scenes. Unlike methods such as SGTR [27] and those discussed in [16], our approach leverages multi-scale representations to accurately delineate subtle relationships.

In addition, the proposed THYME approach incorporates a cyclic temporal refinement mechanism to ensure continuity

across video frames. As described in Sec. IV-C and motivated by the design rationale in [33], the cyclic attention module connects the final frame back to the first. This design reinforces long-range temporal dependencies and mitigates challenges such as transient occlusions. As a result, our approach achieves more balanced scene graph representations, reducing bias toward frequently occurring relationships and enhancing the detection of rare but meaningful interactions. The effectiveness of these integrated modules is further validated by the experimental results presented in Sec. VI, which are consistent with the findings of previous studies [41], [44]. Furthermore, our method demonstrates strong generalizability across diverse viewpoints: evaluations on both ground-view and aerial datasets (see Secs. V and VI) show that our approach adapts well to varying scenarios, thus broadening the applicability of VidSGG.

#### IV. THE PROPOSED THYME APPROACH

In this section, we introduce the proposed Temporal Hierarchical Cyclic Interactivity Model for Video Scene Graphs approach, which leverages a hierarchical structure for temporal modeling while preserving coherent temporal dynamics for VidSGG. In our formulation, a video scene graph is defined as  $\mathcal{G} = (\mathcal{V}, \mathcal{E})$ , where each node  $S_i \in \mathcal{V}$  represents an object tracked throughout the video with a unified feature, and each edge  $(S_i, S_j) \in \mathcal{E}$  is labeled with a predicate  $p \in \mathcal{C}_p$  that describes the relationship between objects.

The proposed THYME approach unfolds in four stages. First, *per frame feature extraction* generates robust object embeddings for each frame. Next, *hierarchical feature aggregation* progressively builds layered spatial representations that capture fine-grained details. This is followed by cyclic temporal refinement, which ensures consistent temporal dynamics across

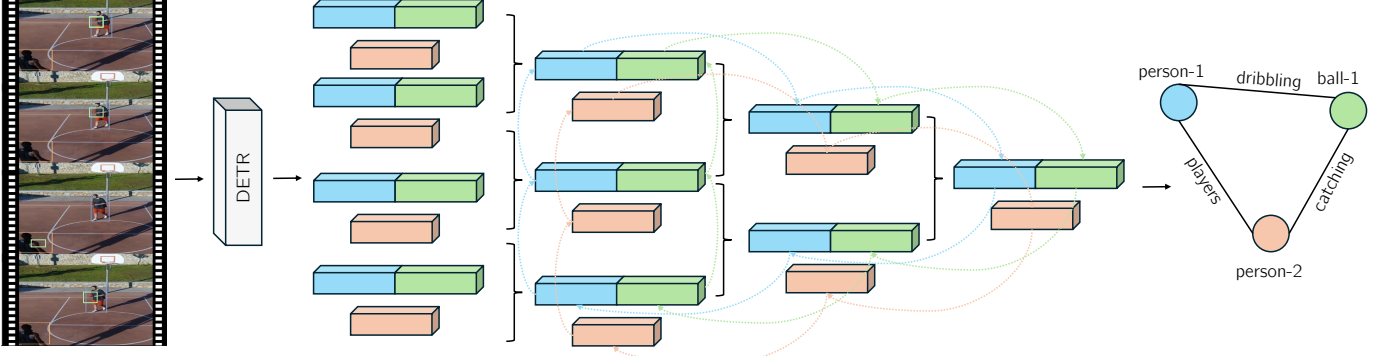


Fig. 3: Overview of the Hierarchical Cyclic Scene Graph approach for Video Scene Graph Generation (VidSGG). Our approach begins by extracting per-frame features using a DETR [1] detector. These features are then hierarchically aggregated into intermediate graphs that capture spatial relationships at various levels of abstraction. A transformer-based cyclic attention mechanism [33] refines these graphs over time, iteratively updating and aligning object representations. Finally, the refined features are integrated into a comprehensive scene graph that encapsulates spatial and temporal object relationships. (Best viewed in colors)

video frames. Finally, these cues are integrated through *scene graph construction* to yield a video scene graph  $\mathcal{G} = (\mathcal{V}, \mathcal{E})$  that models the relationships between objects over time.

#### A. Per-Frame Feature Extraction

Given an input video  $\{I_t\}_{t=1}^T$ , where each frame  $I_t \in \mathbb{R}^{H_0 \times W_0 \times 3}$ , we employ the DETR [1] object detector to extract the features of the object. For each frame  $t$ , the detector produces  $N_t$  object query embeddings  $\{q_i^{(t)} \in \mathbb{R}^{d_0}\}_{i=1}^{N_t}$ , where  $d_0$  denotes the feature dimensionality. These embeddings encode both object appearance and spatial layout. We formally define the set of per-frame object instances as  $V_t = \{S_i^{(t)} \mid S_i^{(t)} \equiv q_i^{(t)}\}$ , where  $S_i^{(t)}$  is the feature of object  $i$  in frame  $t$ .

#### B. Hierarchical Feature Aggregation

To capture intra-frame dynamics, we refine per-frame features using a hierarchical aggregation strategy. Specifically, we initialize each object's feature as  $\mathcal{F}_t^{(0)}(S_i^{(t)}) = q_i^{(t)}$  for every per-frame object  $S_i^{(t)}$  in frame  $t$ , as described in Sec. IV-A.

At each hierarchical level  $l \in \{1, \dots, L_h\}$ , where  $L_h$  is the number of levels, the feature of  $S_i^{(t)}$  is updated by aggregating information from its neighborhood. Specifically, the neighborhood comprises all objects in the frame  $t$ , i.e.,  $\mathcal{N}(S_i^{(t)}) = \mathcal{V}_t$ . Formally, an attention mechanism computes the relevance score between subject  $S_i^{(t)}$  and each object  $S_j^{(t)} \in \mathcal{N}(S_i^{(t)})$ , as defined in Eqn. (1).

$$a_{ij}^{(t)} = \frac{\exp(\mathcal{F}_t^{(l-1)}(S_i^{(t)}) \cdot \mathcal{F}_t^{(l-1)}(S_j^{(t)}))}{\sum_{S_k^{(t)} \in \mathcal{N}(S_i^{(t)})} \exp(\mathcal{F}_t^{(l-1)}(S_i^{(t)}) \cdot \mathcal{F}_t^{(l-1)}(S_k^{(t)}))}. \quad (1)$$

Then, the feature of  $S_i^{(t)}$  at level  $l$  is updated via Eqn. (2).

$$\mathcal{F}_t^{(l)}(S_i^{(t)}) = \sigma \left( \sum_{S_j^{(t)} \in \mathcal{N}(S_i^{(t)})} a_{ij}^{(t)} \left( W^{(l)} \mathcal{F}_t^{(l-1)}(S_j^{(t)}) + b^{(l)} \right) \right), \quad (2)$$

where  $W^{(l)} \in \mathbb{R}^{d_l \times d_{l-1}}$  and  $b^{(l)} \in \mathbb{R}^{d_l}$  are learnable parameters, and  $\sigma(\cdot)$  represents the ReLU activation function.

#### C. Temporal Refinement via Cyclic Attention

To capture inter-frame dynamics, we refine high-level features using a transformer encoder with cyclic attention [33]. For each tracked object  $S_i$  (i.e., its unified trajectory across frames), we construct a temporal sequence  $\{X_{t'}(S_i)\}_{t'=1}^{T'}$ , where each element is given by  $X_{t'}(S_i) = \mathcal{F}_{t'}^{(L_h)}(S_i)$ . Here,  $T'$  represents the number of time steps after temporal pooling, which may differ from  $T$ . Specifically, the extracted features are then projected into query, key, and value spaces using learnable matrices  $W^Q$ ,  $W^K$ , and  $W^V$ , as defined in Eqn. (3).

$$\begin{aligned} Q_{t'}(S_i) &= W^Q X_{t'}(S_i), \\ K_{t'}(S_i) &= W^K X_{t'}(S_i), \\ V_{t'}(S_i) &= W^V X_{t'}(S_i). \end{aligned} \quad (3)$$

The cyclic attention is then computed as defined in Eqn. (4).

$$CA_{t'}(S_i) = \sum_{\tau=0}^{T'-1} \alpha_{t',\tau}(S_i) V_{(t'+\tau) \bmod T'}(S_i), \quad (4)$$

where the attention weights are computed using Eqn. (5).

$$\alpha_{t',\tau}(S_i) = \frac{\exp\left(\frac{Q_{t'}(S_i) \cdot K_{(t'+\tau) \bmod T'}(S_i)}{\sqrt{d_a}}\right)}{\sum_{\tau'=0}^{T'-1} \exp\left(\frac{Q_{t'}(S_i) \cdot K_{(t'+\tau') \bmod T'}(S_i)}{\sqrt{d_a}}\right)}. \quad (5)$$

In Eqn. (5), the modulo operation enforces a cyclic structure, allowing the last time step to attend to the first. In particular, the cyclic attention output is then integrated with the original features through a transformer encoder block, which applies Layer Normalization (LN) and a position-wise feedforward network, resulting in the refined object feature  $\hat{\mathcal{F}}(S_i) \in \mathbb{R}^{d_{L_h}}$ .

#### D. Scene Graph Construction

We construct the video scene graph  $\mathcal{G} = (\mathcal{V}, \mathcal{E})$  using unified object representations, where  $\mathcal{V} = \{S_i \mid \hat{\mathcal{F}}(S_i) \in \mathbb{R}^{d_{L_h}}\}$ . For each pair of objects  $(S_i, S_j)$ , a predicate  $r_{ij} \in \mathcal{C}_r$  is predicted.

To extract relation representations, we leverage self-attention outputs from the DETR decoder. At each decoder layer  $k \in \{1, \dots, L_d\}$ , where  $L_d$  is the total number of layers, the query and the key matrices  $Q^k, K^k \in \mathbb{R}^{N \times d_{\text{model}}}$  are projected using

the learnable parameters  $W_S^k$  and  $W_O^k$ , which form the representation of the relationship  $R_a^k = [Q^k W_S^k; K^k W_O^k]$ . From the final decoder layer, we obtain  $R_z = [Z^{L_d} W_S; Z^{L_d} W_O]$ , where  $Z^{L_d} \in \mathbb{R}^{N \times d_{\text{model}}}$  is the final object query embeddings.

These relation representations are further refined through a gating mechanism, following the method in [16]. Specifically, for each decoder layer  $k$ , the gating coefficient is computed as  $g_a^k = \sigma(R_a^k W_G)$ , while for the final layer, it is given by  $g_z = \sigma(R_z W_G)$ , where  $W_G$  is a shared weight matrix. Finally, the predicted scene graph is obtained as defined in Eqn. (6).

$$\hat{G} = \sigma \left( \text{MLP}_{\text{rel}} \left( \sum_{k=1}^{L_d} (g_a^k \odot R_a^k) + g_z \odot R_z \right) \right), \quad (6)$$

where  $\odot$  denotes element-wise multiplication and  $\text{MLP}_{\text{rel}}$  outputs scores over predicate classes for each object pair.

### E. Loss Function

Following [32], we adopt Focal Loss for edge classification. Let  $\tilde{p}_t(\mathcal{F}_t^{(l)}(S_i^{(t)}))$  denote the predicted probability for the feature  $\mathcal{F}_t^{(l)}(S_i^{(t)})$ , where  $\alpha_t$  is a balancing factor, and  $\gamma$  controls the focusing effect. Mathematically, the loss at level  $l$  is defined in Eqn. (7).

$$\mathcal{L}(\mathcal{F}_t^{(l)}(S_i^{(t)})) = -\alpha_t \left( 1 - \tilde{p}_t(\mathcal{F}_t^{(l)}(S_i^{(t)})) \right)^\gamma \log(\tilde{p}_t(\mathcal{F}_t^{(l)}(S_i^{(t)}))). \quad (7)$$

The total loss across hierarchical levels is computed by aggregating the losses at each level, as defined in Eqn. (8).

$$\mathcal{L}_{\text{total}} = \sum_{l=1}^{L_h} \mathcal{L}(\mathcal{F}_t^{(l)}(S_i^{(t)})). \quad (8)$$

## V. PROPOSED AEROEYE-V1.0 DATASET

### A. The Previous Datasets and Their Limitations

The AeroEye dataset [33] offers valuable annotations for object interactions and spatial relationships, but it has notable limitations. Although it captures object positions and interactions, it omits key visual features such as color, size, and shape, and it does not provide information about the environmental context, often referred to as the situation in which the objects are placed. Moreover, it fails to differentiate between various types of interactions and relationships. For example, when one car tows another, explicitly labeling the interaction as “towing” and the relationship as “assisting” clarifies the dynamics.

Similarly, the ASPIRe dataset [32] introduces five distinct types of interactivity, a promising step toward richer annotations. However, its focus on ground-view scenes captured from a third-person perspective excludes aerial or drone viewpoints, which are increasingly vital for comprehensive scene analysis.

To address these limitations, our new AeroEye-v1.0 dataset introduces five annotation types: Appearance, Situation, Position, Interaction, and Relation. These enhancements support richer representations of object behaviors, spatial relationships, interactions, and environmental contexts, thereby facilitating the creation of more comprehensive video scene graphs.

### B. Our Dataset Annotation

AeroEye-v1.0 builds on the AeroEye [33] dataset. In particular, AeroEye-v1.0 includes five distinct interactivity types defined in [32]. (i) *Appearance* annotations describe the visual characteristics, including type (e.g., sedan, SUV), color, size (e.g., short, long), and shape. (ii) *Situation* annotations provide contextual information about the environment in which objects interact, such as the setting (urban, rural), weather conditions (sunny, rainy), time of day (day, night), and events (e.g., traffic congestion, accidents, floods). (iii) *Position* annotations describe the spatial relationships between objects, for example, “in front of”, or “beside”. (iv) *Interaction* annotations capture the dynamic actions between objects, such as “crashing”, “towing”, or “overtaking”, thereby highlighting how objects behave relative to one another over time. (v) *Relation* annotations define the functional connections between objects, such as “assisting”, “escorting”, or “guiding”. These annotations clarify the roles and relationships between objects.

In our annotation process, every frame is annotated so that each object, represented by a bounding box, is assigned appearance and situation annotations. When spatial relationships between objects (i.e., their positions) are annotated, additional interaction and relation annotations further detail their relationships, as illustrated in Fig. 4. However, in parked cars, where the positions are recorded as “in front of”, “behind”, or “next to”, no interaction or relation annotations are applied.

### C. The Dataset Statistics

The AeroEye-v1.0 dataset comprises 2,260 videos spanning 261,503 frames, captured by drones in various urban, suburban and rural environments. This varied data acquisition provides a rich foundation for analyzing dynamic scenes from multiple perspectives. The dataset includes 56 unique object categories, with over 2 million bounding boxes and corresponding tracking annotations. Each bounding box is enriched with appearance and situation annotations that capture every visual detail of the objects and the environmental context.

Specifically, the AeroEye-v1.0 dataset provides 157 appearance predicates and 128 situation predicates. Individually, spatial annotations between pairs of objects are annotated using 135 distinct position predicates, resulting in approximately 752K position annotations. In addition, dynamic interactions are captured with 142 unique interaction predicates, yielding approximately 318K interaction annotations, while 125 unique relation predicates result in roughly 178K relation annotations.

Significantly, AeroEye-v1.0 surpasses previous VidSGG benchmarks across all key dimensions, including the number of videos, annotated frames, object and predicate vocabulary, and viewpoint diversity, i.e., aerial, oblique, and ground perspectives. In addition, AeroEye-v1.0 is the only drone-captured video dataset to annotate all five types of interactivity necessary for fine-grained VidSGG. As detailed in Table I, these advantages position our AeroEye-v1.0 dataset as the most comprehensive and challenging dataset to advance dynamic scene graph generation in aerial environments.



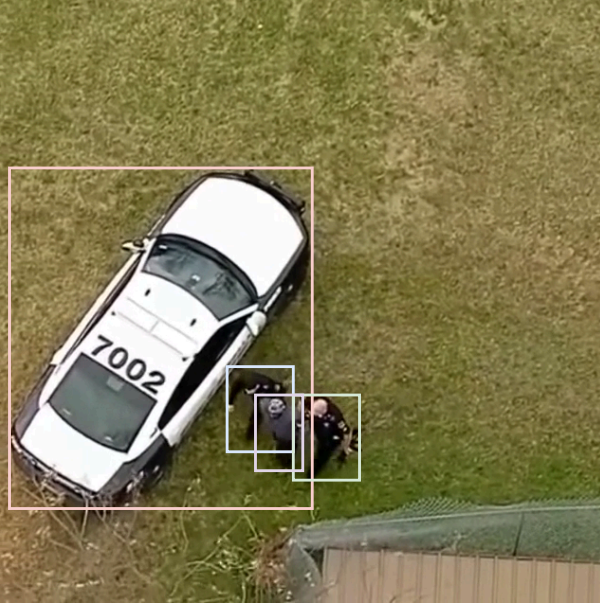


Fig. 4: Example from AeroEye-v1.0. The scene graph is annotated with nodes denoting objects (bounding boxes), each with appearance and situation annotations. Edges include position annotations (curved arrows), interaction annotations (straight arrows), and relation annotations (dashed lines). **(Best viewed in colors)**

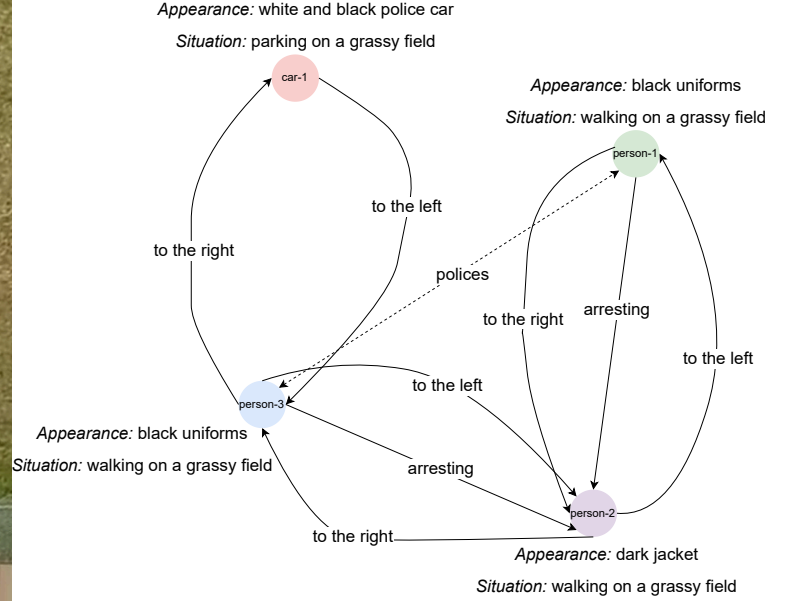


TABLE II: Effect of factor size on R@20 and mR@20 across different interactivity types on the AeroEye-v1.0 dataset. Best scores are **bolded**.

Factor	Interactivity Type	R@20	mR@20
1/4	Appearance	14.12	0.60
	Situation	4.33	0.55
	Position	12.32	0.87
	Interaction	10.87	0.12
	Relation	13.03	0.85
1/2	Appearance	15.22	0.64
	Situation	5.03	0.57
	Position	13.52	0.97
	Interaction	11.87	0.14
	Relation	14.03	0.90
3/4	Appearance	16.48	0.65
	Situation	5.63	0.62
	Position	15.62	1.06
	Interaction	13.17	0.16
	Relation	16.13	0.95
Full	Appearance	<b>16.52</b>	<b>0.68</b>
	Situation	<b>5.53</b>	<b>0.61</b>
	Position	<b>15.52</b>	<b>1.05</b>
	Interaction	<b>13.07</b>	<b>0.16</b>
	Relation	<b>16.03</b>	<b>0.95</b>

## VI. EXPERIMENTS

### A. Implementation Details

**Datasets.** We evaluate on two challenging and diverse datasets: ASPIRe [32] and AeroEye-v1.0. The ASPIRe dataset comprises dynamic videos captured in real-world ground-level scenarios and includes rich annotations across five interactivity types, i.e., Appearance, Situation, Position, Interaction, and Relation, making it a strong benchmark for ground-view scene graph generation. In contrast, the AeroEye-v1.0 dataset contains aerial videos that pose unique challenges, such as high object density, varying object scales, and complex spatial relationships.

**Metrics.** Following [52], [32], [33], we evaluate methods using Recall (R) and mean Recall (mR) at multiple thresholds,

specifically, predictions from the *top-20*, *top-50*, and *top-100*.

### B. Ablation Study

1) *Number of Hierarchical Levels:* Table II presents an ablation study on the number of hierarchical levels of THYME, demonstrating that deeper aggregation significantly improves the model’s ability to fuse multi-scale spatial features and capture temporal information between interactivity types on AeroEye-v1.0. For example, using only 1/4 of the full hierarchy yields 14.12% R@20 and 0.60% mR@20 in the Appearance category. In contrast, using the full depth boosts these metrics to 16.52% and 0.68%, highlighting the benefits of richer feature representations. Similar trends are observed in the Situation category (R@20 increasing from 4.33% to 5.53%), and in double-actor attributes: Position (from 12.32% to 15.52%), Interaction (from 10.87% to 13.07%), and Relation (from 13.03% to 16.03%). In particular, most performance gains occur when increasing from 1/4 to 3/4 of the full depth, with only marginal improvements beyond that point. It suggests the existence of an optimal hierarchical depth that balances fine-grained detail extraction with global context aggregation without incurring diminishing returns. These findings highlight the role of hierarchical structure in our THYME approach for dynamic scene graph generation, enabling the model to effectively capture inter-object dynamics through progressively refined feature representations across abstraction levels.

2) *Temporal Attention Mechanism:* The ablation results in Table III, based on experiments with the temporal attention mechanism, show that cyclic temporal attention consistently outperforms standard self-attention across all interactivity types. For example, in the Appearance category, replacing standard attention with cyclic attention increases R@20 from 15.12% to 16.52% and mR@20 from 0.65% to 0.68%. Similar improvements are observed in Situation (R@20: 4.83% to 5.53%, mR@20: 0.59% to 0.61%), Position (13.42% to

TABLE III: Comparison between attention mechanisms on R@20 and mR@20 across interactivity types on the AeroEye-v1.0 dataset. Best scores are **bolded**.

Mechanism	Interactivity Type	R@20	mR@20
Standard Attention	Appearance	15.12	0.65
	Situation	4.83	0.59
	Position	13.42	0.92
	Interaction	11.07	0.14
	Relation	14.03	0.85
Cyclic Attention	Appearance	<b>16.52</b>	<b>0.68</b>
	Situation	<b>5.53</b>	<b>0.61</b>
	Position	<b>15.52</b>	<b>1.05</b>
	Interaction	<b>13.07</b>	<b>0.16</b>
	Relation	<b>16.03</b>	<b>0.95</b>

TABLE IV: Effect of different window sizes on R@20 and mR@20 across interactivity types on the AeroEye-v1.0 dataset. Best scores are **bolded**.

Window Size	Interactivity Type	R@20	mR@20
1/2	Appearance	15.32	0.66
	Situation	5.03	0.59
	Position	14.02	0.97
	Interaction	12.07	0.15
	Relation	15.03	0.90
3/4	Appearance	<b>16.52</b>	<b>0.68</b>
	Situation	<b>5.53</b>	<b>0.61</b>
	Position	<b>15.52</b>	<b>1.05</b>
	Interaction	<b>13.07</b>	<b>0.16</b>
	Relation	<b>16.03</b>	<b>0.95</b>
Full	Appearance	16.22	0.67
	Situation	5.43	0.60
	Position	15.22	1.03
	Interaction	12.77	0.15
	Relation	15.73	0.93

15.52%, 0.92% to 1.05%), Interaction (11.07% to 13.07%, 0.14% to 0.16%), and Relation (14.03% to 16.03%, 0.85% to 0.95%). These gains, ranging from approximately 1.4% to 2.0% percentage points in R@20 and the corresponding increases in mR@20, underscore the effectiveness of cyclic attention in modeling long-range temporal dependencies and capturing periodic patterns over time. By mitigating the loss of crucial contextual information, this mechanism enhances the model’s ability to generate more discriminative video scene graphs.

3) *Temporal Window Size*: Table IV presents an ablation study on temporal window size, showing that increasing temporal context consistently improves both Recall (R@20) and mean Recall (mR@20) across all interactivity types. With a smaller window size of 1, the model achieves lower scores. For example, Appearance registers 15.32% R@20 and 0.66 mR@20, while Position reaches 14.02% and 0.97% mR@20. Expanding the window to 3/4 leads to improved results, with appearance reaching 16.22% R@20 and 0.67% mR@20, and position achieving 15.22% and 1.03% mR@20. These improvements indicate that a greater temporal context enables better feature fusion and more accurate dynamic modeling. Especially, the best performance is achieved with the full window, where Appearance attains 16.52% R@20 and 0.68% mR@20, and Position reaches 15.52% and 1.05% mR@20. Although the performance gains from 3/4 to full window are marginal, the full window setting consistently yields the highest scores. This suggests that capturing the complete temporal context is particularly beneficial for modeling single-actor and

TABLE V: Comparisons of video scene graph generation methods on the ASPIRe dataset. The table reports Recall (R) and mean Recall (mR) at top-20, top-50, and top-100 predictions for five interactivity types: Appearance, Situation, Position, Interaction, and Relation. Evaluated methods include state-of-the-art models (IMP, MOTIFS, VCTree, GPSNet, STTran, and TEMPURA), our previous approaches (HIG and CYCLO), and the proposed THYME.

Method	Interactivity Type	R/mR@20	R/mR@50	R/mR@100
IMP	Appearance	-	-	-
	Situation	-	-	-
	Position	9.70 / 0.49	9.70 / 0.49	9.70 / 0.49
	Interaction	12.79 / 0.08	12.79 / 0.08	12.79 / 0.08
	Relation	11.51 / 0.32	11.51 / 0.32	11.51 / 0.32
MOTIFS	Appearance	-	-	-
	Situation	-	-	-
	Position	6.89 / 0.48	8.49 / 0.38	8.70 / 0.40
	Interaction	8.83 / 0.12	10.33 / 0.12	10.63 / 0.12
	Relation	8.72 / 0.32	10.26 / 0.32	10.55 / 0.32
VCTree	Appearance	-	-	-
	Situation	-	-	-
	Position	4.18 / 0.39	6.75 / 0.40	8.59 / 0.42
	Interaction	6.23 / 0.10	9.58 / 0.10	11.63 / 0.10
	Relation	6.51 / 0.27	9.82 / 0.28	11.51 / 0.28
GPSNet	Appearance	-	-	-
	Situation	-	-	-
	Position	12.89 / 1.26	12.89 / 1.26	12.89 / 1.26
	Interaction	10.89 / 0.11	10.89 / 0.11	10.89 / 0.11
	Relation	9.87 / 0.35	9.87 / 0.35	9.87 / 0.35
HIG (Ours)	Appearance	15.02 / 0.60	18.60 / 0.64	20.11 / 0.65
	Situation	5.01 / 0.56	7.02 / 0.55	12.01 / 0.63
	Position	13.02 / 0.09	24.52 / 1.33	42.33 / 1.13
	Interaction	12.02 / 0.11	24.65 / 0.12	41.65 / 0.14
	Relation	10.26 / 0.29	23.72 / 0.34	41.47 / 0.39
STTran	Appearance	-	-	-
	Situation	-	-	-
	Position	13.52 / 0.51	24.92 / 1.38	42.80 / 1.31
	Interaction	12.27 / 0.14	24.84 / 0.17	41.85 / 0.21
	Relation	12.03 / 0.51	23.93 / 0.81	42.85 / 1.01
CYCLO (Ours)	Appearance	-	-	-
	Situation	-	-	-
	Position	16.32 / 0.97	29.41 / 1.60	48.67 / 1.65
	Interaction	15.27 / 0.20	28.32 / 1.27	46.15 / 2.32
	Relation	18.34 / 0.90	28.17 / 1.70	50.23 / 2.60
TEMPURA	Appearance	-	-	-
	Situation	-	-	-
	Position	13.71 / 0.85	26.07 / 1.45	43.94 / 1.49
	Interaction	12.53 / 0.17	25.03 / 0.22	42.03 / 0.27
	Relation	15.29 / 0.84	24.95 / 1.61	46.44 / 1.52
THYME (Ours)	Appearance	<b>18.23 / 1.07</b>	<b>21.67 / 1.61</b>	<b>23.12 / 2.72</b>
	Situation	<b>6.57 / 0.26</b>	<b>8.64 / 1.76</b>	<b>14.23 / 2.67</b>
	Position	<b>18.52 / 1.22</b>	<b>31.03 / 2.42</b>	<b>50.05 / 2.53</b>
	Interaction	<b>19.52 / 0.32</b>	<b>30.03 / 1.42</b>	<b>48.04 / 2.47</b>
	Relation	<b>21.02 / 1.12</b>	<b>32.03 / 1.82</b>	<b>54.05 / 2.93</b>

double-actor interactivity types in dynamic video scenes.

### C. Comparison with State-of-the-Arts

1) *Performance on ASPIRe*: Table V demonstrates that our THYME approach consistently outperforms state-of-the-art methods on the ASPIRe dataset across interactivity types.

In particular, STTran, which employs a spatio-temporal transformer to model video data, shows notable improvement over earlier baselines. However, its performance on double-actor attributes remains limited, achieving only 13.52% R@20 and 0.51 mR@20 in Position and 12.27% R@20 and 0.14 mR@20 in Interaction. Similarly, TEMPURA builds on STTran by incorporating debiasing mechanisms and uncertainty-aware classification, resulting in modest performance gains. Nevertheless, TEMPURA still struggles to capture the complex temporal dynamics inherent in multi-object relationships.

HIG provides a foundation for our approach by employing a hierarchical structure. Although it improves upon static

TABLE VI: Comparisons of various methods on the AeroEye-v1.0 dataset for video scene graph generation. The table reports Recall (R) and mean Recall (mR) at top-20, top-50, and top-100 predictions across five interactivity types: Appearance, Situation, Position, Interaction, and Relation. Baseline methods (IMP, MOTIFS, VCTree, and GPSNet) are compared with our previous approaches (HIG and CYCLO) and the proposed THYME.

Method	Interactivity Type	R/mR@20	R/mR@50	R/mR@100
IMP	Appearance	-	-	-
	Situation	-	-	-
	Position	8.47 / 0.41	8.52 / 0.39	8.57 / 0.42
	Interaction	11.13 / 0.07	12.03 / 0.08	12.71 / 0.13
	Relation	10.02 / 0.28	10.51 / 0.28	10.00 / 0.28
MOTIFS	Appearance	-	-	-
	Situation	-	-	-
	Position	6.50 / 0.45	7.75 / 0.35	7.83 / 0.38
	Interaction	8.03 / 0.11	9.00 / 0.15	9.54 / 0.17
	Relation	7.92 / 0.31	9.12 / 0.35	9.52 / 0.42
VCTree	Appearance	-	-	-
	Situation	-	-	-
	Position	3.81 / 0.35	5.03 / 0.36	6.51 / 0.38
	Interaction	5.53 / 0.08	7.55 / 0.09	8.79 / 0.12
	Relation	5.82 / 0.25	7.13 / 0.27	8.51 / 0.29
GPSNet	Appearance	-	-	-
	Situation	-	-	-
	Position	11.47 / 0.83	11.23 / 0.95	11.54 / 1.12
	Interaction	9.47 / 0.12	9.53 / 0.15	9.76 / 0.21
	Relation	8.62 / 0.42	8.73 / 0.47	8.97 / 0.53
STTran	Appearance	-	-	-
	Situation	-	-	-
	Position	12.22 / 0.75	21.82 / 1.15	37.22 / 1.05
	Interaction	10.52 / 0.08	20.52 / 0.10	36.52 / 0.10
	Relation	8.52 / 0.22	18.52 / 0.32	35.52 / 0.42
HIG (Ours)	Appearance	14.51 / 0.55	17.62 / 0.62	19.15 / 0.67
	Situation	4.53 / 0.57	6.55 / 0.62	10.58 / 0.72
	Position	12.51 / 0.85	22.53 / 1.26	38.72 / 1.73
	Interaction	11.57 / 0.19	21.95 / 0.21	38.14 / 0.32
	Relation	9.57 / 0.25	20.54 / 0.36	37.58 / 0.35
TEMPURA	Appearance	-	-	-
	Situation	-	-	-
	Position	13.22 / 0.82	23.22 / 1.25	39.22 / 1.37
	Interaction	11.81 / 0.12	21.80 / 0.14	37.80 / 0.16
	Relation	11.47 / 0.33	21.53 / 0.45	40.42 / 0.76
CYCLO	Appearance	-	-	-
	Situation	-	-	-
	Position	13.52 / 0.75	25.03 / 1.35	40.12 / 1.40
	Interaction	12.61 / 0.14	23.05 / 0.23	38.82 / 0.24
	Relation	14.51 / 0.83	22.52 / 1.41	45.38 / 1.55
THYME (Ours)	Appearance	<b>16.52 / 0.68</b>	<b>19.53 / 0.72</b>	<b>21.07 / 0.83</b>
	Situation	<b>5.53 / 0.61</b>	<b>7.57 / 0.76</b>	<b>11.51 / 0.85</b>
	Position	<b>15.52 / 1.05</b>	<b>26.03 / 1.45</b>	<b>42.03 / 2.15</b>
	Interaction	<b>13.07 / 0.16</b>	<b>24.53 / 1.22</b>	<b>41.53 / 2.26</b>
	Relation	<b>16.03 / 0.95</b>	<b>26.53 / 1.74</b>	<b>48.03 / 2.38</b>

modeling approaches, HIG exhibits limitations in achieving temporal consistency and producing balanced predictions across frequent and rare predicate classes. Furthermore, CYCLO advances this further by introducing cyclic temporal refinement, which improves the temporal modeling of dynamic interactions. However, CYCLO fails to capture multi-scale spatial context and long-range temporal dependencies within video scenes.

THYME distinguishes itself by combining cyclic temporal refinement with hierarchical feature aggregation. This dual mechanism enables the extraction of features at multiple levels of abstraction, enhancing temporal consistency and spatial context modeling. Therefore, THYME achieves significant performance gains. For single-actor attributes, it records 18.23% R@20 and 1.07 mR@20 in Appearance, and 6.57% R@20 and 0.26 mR@20 in Situation, clearly outperforming STTran, TEMPURA, and HIG. The improvements are even more pronounced for double-actor attributes, where THYME achieves 18.52% R@20 and 1.22 mR@20 in Position, 19.52% R@20

and 0.32 mR@20 in Interaction, and 21.02% R@20 and 1.12 mR@20 in Relation, surpassing HIG and CYCLO.

These improvements, particularly in mean Recall, highlight THYME’s ability to generate more balanced and discriminative predictions across varying predicate frequencies, resulting in more comprehensive scene graphs, as illustrated in Fig. 5.

2) *Performance on AeroEye-v1.0.*: The experimental results in Table VI demonstrate a progressive improvement in dynamic scene graph generation performance on the AeroEye-v1.0 dataset, with our proposed THYME approach achieving the highest scores across most interactivity types. Traditional methods such as IMP, MOTIFS, VCTree, and GPSNet primarily rely on static or limited spatio-temporal cues. As a result, they exhibit relatively low Recall and mean Recall values, particularly in capturing dynamic interactions. For example, IMP achieves only 8.47% Recall for Position and 11.13% for Interaction at R@20, while VCTree and GPSNet show only modest improvements. These results highlight the inherent limitations of prior methods that fail to utilize temporal context.

Transformer-based methods, such as STTran, show noticeable improvements over traditional methods, achieving 12.22% R@20 in Position and 10.52% in Interaction. However, STTran struggles with complex interactivity, as indicated by its low Relation score of 8.52% R@20. In addition, HIG promotes dynamic interactivity modeling with 12.51% R@20 in Position and 11.57% in Interaction, along with improved mR. Moreover, TEMPURA slightly improves performance, reaching 13.22% R@20 in Position and 11.47% in Relation. Despite these gains, existing models face challenges in handling long-tail predicate distributions and capturing subtle interactivity transitions.

Notably, THYME achieves substantial improvements across all interactivity: 16.52% R@20 in Appearance, 5.53% in Situation, and significantly higher scores for double-actor attributes (15.52% in Position, 13.07% in Interaction, and 16.03% in Relation). In addition, the mean Recall values also improve considerably, with THYME reaching 1.05% for Position, 0.16% for Interaction, and 0.95% for Relation at mR@20. These results outperform the second-best method (e.g., CYCLO) by 2–3% in terms of Recall on double-actor attributes, enabling the generation of more comprehensive scene graphs for drone-captured video, as further illustrated in Fig. 6.

#### D. Qualitative Results

In Fig. 5, HIG and CYCLO encounter difficulties when objects are occluded or missing from the scene (e.g., *person-3* and *ball-1*). Due to its lack of temporal refinement, HIG fails to predict subsequent relationships once an object disappears. HIG cannot effectively leverage prior context to generate accurate predictions when the object is no longer visible, as illustrated in Fig. 5a. CYCLO, on the other hand, attempts to address this issue by relying on periodic interactions, following sequences such as *catching* to *dribbling* to *hitting*. However, this reliance on fixed interaction patterns makes it vulnerable to errors when key objects like *ball-1* are occluded, as the model struggles to adapt to disruptions in the expected sequence, as shown in Fig. 5b. In contrast, our approach offers a dynamic solution. When *ball-1* disappears from the scene, THYME



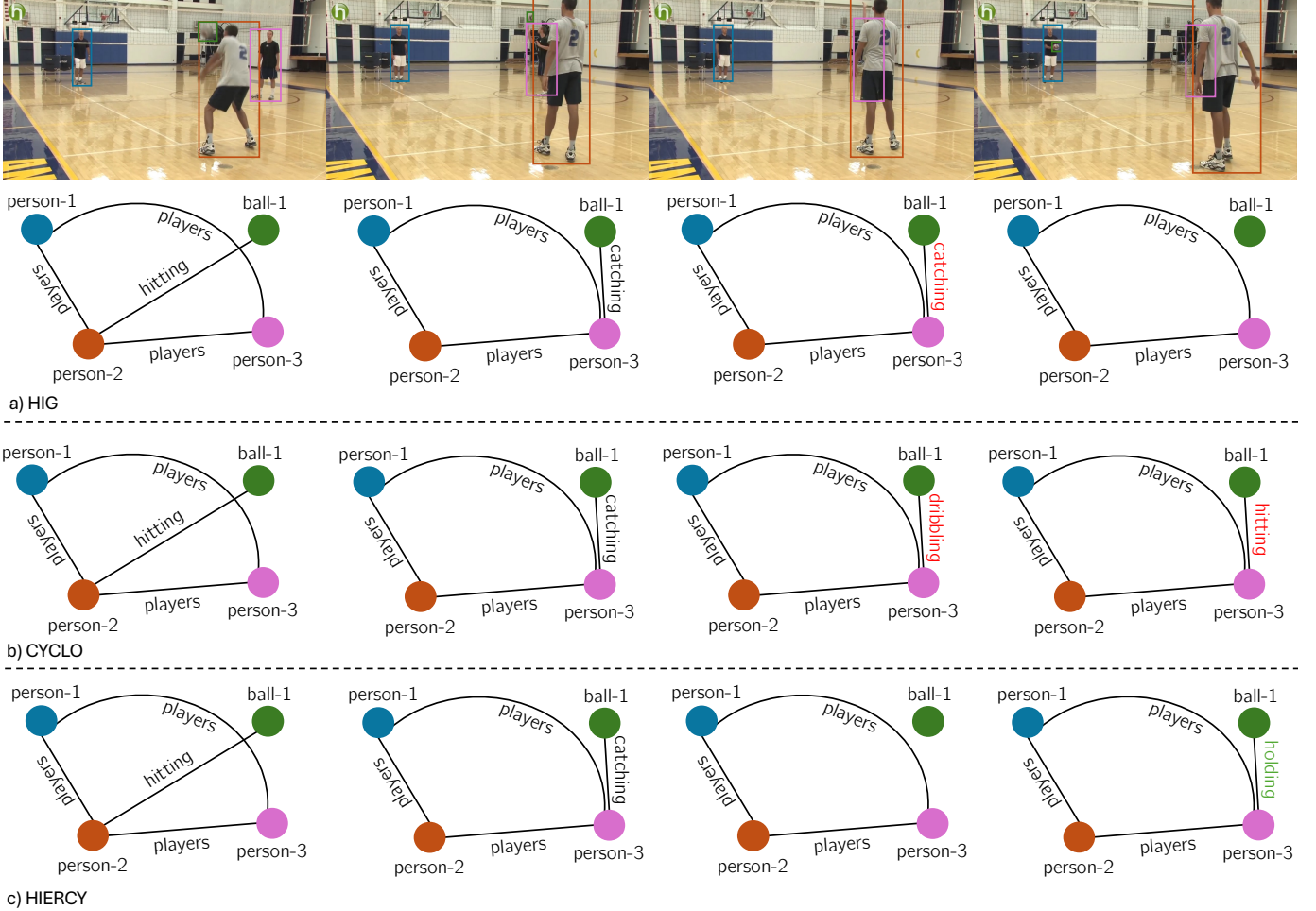


Fig. 5: Qualitative comparison on the ASPIRe dataset. Green edges denote correct predictions, while red edges is incorrect predictions. (Best viewed in colors)

employs an advanced tracking mechanism enabled by its hierarchical structure and leverages cyclic attention to maintain a refined understanding of the object’s temporal trajectory.

In Fig. 6, the scenario where a police car is chasing another car captured from a drone view, HIG struggles to capture the evolving dynamics, particularly the shift in relative position between the two vehicles. As the police car changes from being behind to alongside the other car, HIG fails to recognize this change, continuing to predict “chasing” without updating to “approaching” or anticipating the “crashing” event. On the other hand, CYCLO relies on periodic interaction patterns and struggles with predicting the correct position between the cars. This leads to an incorrect shift from “approaching” back to “chasing”, failing to capture the nuanced interactions and missing the prediction of the crash. THYME, however, successfully tracks the changing positions and speed of the vehicles, updating its prediction history from “chasing” to “approaching” as the cars move closer. THYME’s cyclic temporal refinement allows it to predict the progression of interactions accurately, ultimately forecasting the “crashing” event by leveraging both spatial and temporal features across multiple levels of abstraction, outperforming HIG and CYCLO in capturing the dynamic changes in the video scene.

## VII. CONCLUSION

In this work, we have introduced the THYME approach, which integrates hierarchical feature aggregation with cyclic temporal refinement to capture multi-scale spatial details and maintain temporal consistency in video scene graph generation. In addition, we have presented AeroEye-v1.0, a novel aerial video dataset enriched with comprehensive annotations across appearance, situation, position, interaction, and relation. Moreover, our extensive experiments on the ASPIRe and AeroEye-v1.0 datasets have demonstrated that the proposed THYME approach significantly outperforms existing state-of-the-art methods, yielding more accurate and consistent scene graph representations in ground-view and aerial scenarios.

Future work can include integrating multimodal cues, such as audio and textual information, to enrich the scene representations and exploring domain adaptation techniques to extend our approach to a broader range of real-world scenarios. In addition, our objective is to investigate advanced mechanisms for bias reduction and the incorporation of additional contextual cues to handle long-tail predicate distributions better.

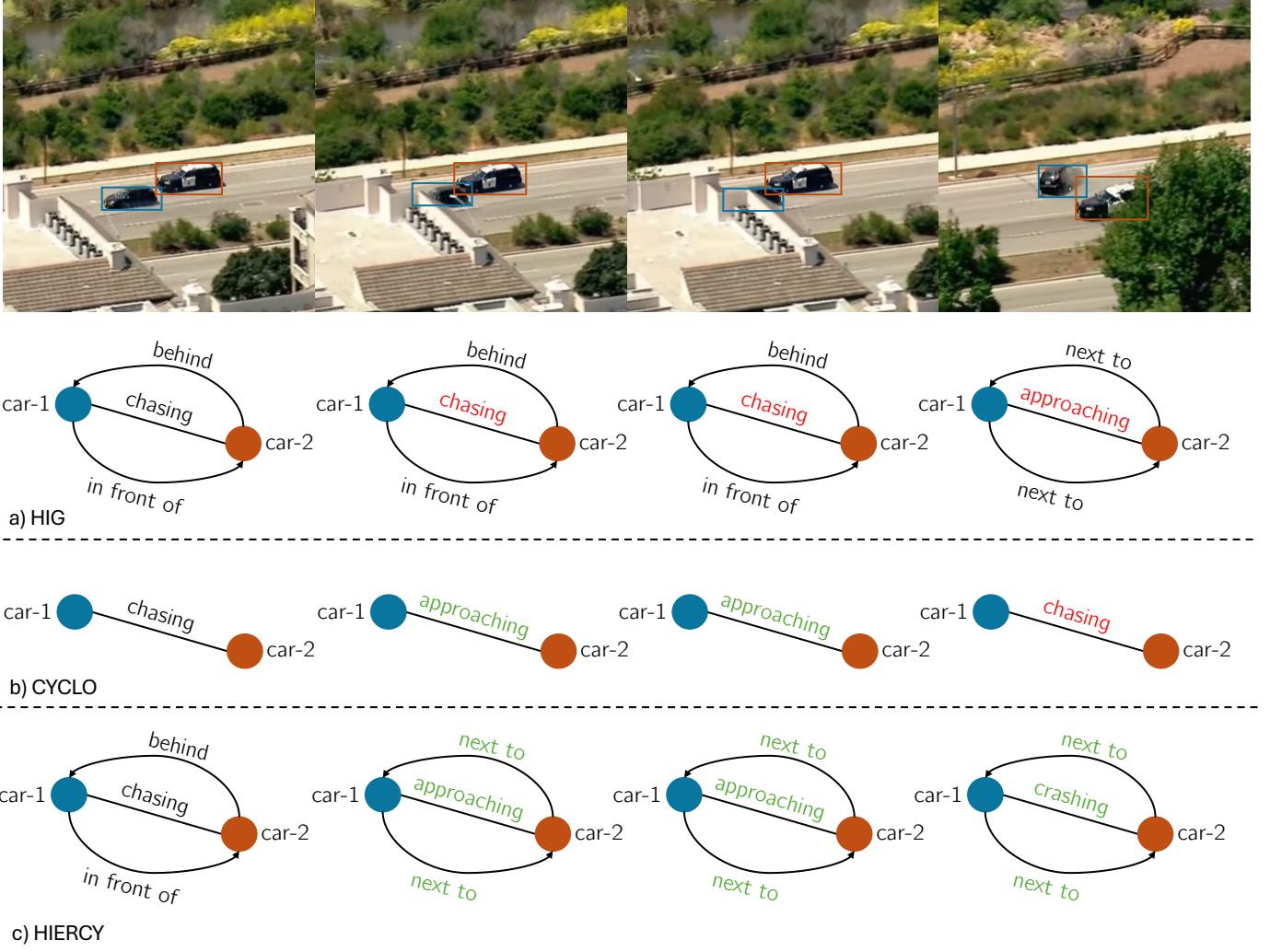


Fig. 6: Qualitative comparison on the AeroEye-v1.0 dataset. Green edges is correct predictions, while red edges is incorrect predictions. (Best viewed in colors)

## REFERENCES

- [1] Nicolas Carion, Francisco Massa, Gabriel Synnaeve, Nicolas Usunier, Alexander Kirillov, and Sergey Zagoruyko. End-to-end object detection with transformers. In *European conference on computer vision*, pages 213–229. Springer, 2020. 6
- [2] Orcun Cetintas, Guillem Brasó, and Laura Leal-Taixé. Unifying short and long-term tracking with graph hierarchies. In *Proceedings of the IEEE/CVF Conference on Computer Vision and Pattern Recognition*, pages 22877–22887, 2023. 2
- [3] Zhanwen Chen, Saed Rezayi, and Sheng Li. More knowledge, less bias: Unbiasing scene graph generation with explicit ontological adjustment. In *Proceedings of the IEEE/CVF Winter Conference on Applications of Computer Vision*, pages 4023–4032, 2023. 3
- [4] Yuren Cong, Wentong Liao, Hanno Ackermann, Bodo Rosenhahn, and Michael Ying Yang. Spatial-temporal transformer for dynamic scene graph generation. In *Proceedings of the IEEE/CVF international conference on computer vision*, pages 16372–16382, 2021. 3
- [5] Yuren Cong, Michael Ying Yang, and Bodo Rosenhahn. Reltr: Relation transformer for scene graph generation. *IEEE Transactions on Pattern Analysis and Machine Intelligence*, 45(9):11169–11183, 2023. 2, 4
- [6] Dima Damen, Hazel Doughty, Giovanni Maria Farinella, Antonino Furnari, Evangelos Kazakos, Jian Ma, Davide Moltisanti, Jonathan Munro, Toby Perrett, Will Price, et al. Rescaling egocentric vision: Collection, pipeline and challenges for epic-kitchens-100. *International Journal of Computer Vision*, pages 1–23, 2022. 3
- [7] Long Hoang Dang, Thao Minh Le, Vuong Le, and Truyen Tran. Hierarchical object-oriented spatio-temporal reasoning for video question answering. *arXiv preprint arXiv:2106.13432*, 2021. 2
- [8] Jeonghyeok Do and Munchul Kim. Skateformer: skeletal-temporal transformer for human action recognition. In *European Conference on Computer Vision*, pages 401–420. Springer, 2024. 2
- [9] Shengyu Feng, Hesham Mostafa, Marcel Nassar, Somdeb Majumdar, and Subarna Tripathi. Exploiting long-term dependencies for generating dynamic scene graphs. In *Proceedings of the IEEE/CVF Winter Conference on Applications of Computer Vision*, pages 5130–5139, 2023. 2, 3, 4
- [10] Difei Gao, Luowei Zhou, Lei Ji, Linciao Zhu, Yi Yang, and Mike Zheng Shou. Mist: Multi-modal iterative spatial-temporal transformer for long-form video question answering. In *Proceedings of the IEEE/CVF conference on computer vision and pattern recognition*, pages 14773–14783, 2023. 2
- [11] Gege Gao, Weiyang Liu, Anpei Chen, Andreas Geiger, and Bernhard Schölkopf. Graphdreamer: Compositional 3d scene synthesis from scene graphs. *arXiv preprint arXiv:2312.00093*, 2023. 3
- [12] Zeeshan Hayder and Xuming He. Dsgg: Dense relation transformer for an end-to-end scene graph generation. In *Proceedings of the IEEE/CVF Conference on Computer Vision and Pattern Recognition*, pages 28317–28326, 2024. 2, 3, 4
- [13] Tao He, Lianli Gao, Jingkuan Song, and Yuan-Fang Li. Toward a unified transformer-based framework for scene graph generation and human-object interaction detection. *IEEE Transactions on Image Processing*, 32:6274–6288, 2023. 2, 4
- [14] Drew A Hudson and Christopher D Manning. Gqa: A new dataset for real-world visual reasoning and compositional question answering. In *Proceedings of the IEEE/CVF conference on computer vision and pattern recognition*, pages 6700–6709, 2019. 3
- [15] Guangyu Huo, Yong Zhang, Boyue Wang, Junbin Gao, Yongli Hu, and Baocai Yin. Hierarchical spatio-temporal graph convolutional networks and transformer network for traffic flow forecasting. *IEEE Transactions*

- on Intelligent Transportation Systems, 24(4):3855–3867, 2023. 2
- [16] Jinbae Im, JeongYeon Nam, Nokyoung Park, Hyungmin Lee, and Seunghyun Park. Egtr: Extracting graph from transformer for scene graph generation. In *Proceedings of the IEEE/CVF Conference on Computer Vision and Pattern Recognition*, pages 24229–24238, 2024. 2, 3, 4, 5, 7
- [17] Jingwei Ji, Ranjay Krishna, Li Fei-Fei, and Juan Carlos Niebles. Action genome: Actions as compositions of spatio-temporal scene graphs. In *Proceedings of the IEEE/CVF Conference on Computer Vision and Pattern Recognition*, pages 10236–10247, 2020. 2, 3
- [18] Xiaosong Jia, Penghao Wu, Li Chen, Yu Liu, Hongyang Li, and Junchi Yan. Hdgt: Heterogeneous driving graph transformer for multi-agent trajectory prediction via scene encoding. *IEEE transactions on pattern analysis and machine intelligence*, 45(11):13860–13875, 2023. 2
- [19] Tianlei Jin, Fangtai Guo, Qiwei Meng, Shiqiang Zhu, Xiangming Xi, Wen Wang, Zonghao Mu, and Wei Song. Fast contextual scene graph generation with unbiased context augmentation. In *Proceedings of the IEEE/CVF Conference on Computer Vision and Pattern Recognition*, pages 6302–6311, 2023. 3, 4
- [20] WeiKe Jin, Zhou Zhao, Pengcheng Zhang, Jieming Zhu, Xiuqiang He, and Yueting Zhuang. Hierarchical cross-modal graph consistency learning for video-text retrieval. In *Proceedings of the 44th International ACM SIGIR Conference on research and development in information retrieval*, pages 1114–1124, 2021. 2
- [21] Siddhesh Khandelwal, Mohammed Suhail, and Leonid Sigal. Segmentation-grounded scene graph generation. In *Proceedings of the IEEE/CVF International Conference on Computer Vision*, pages 15879–15889, 2021. 3
- [22] Kibum Kim, Kanghoon Yoon, Jaehyeong Jeon, Yeonjun In, Jinyoung Moon, Donghyun Kim, and Chanyoung Park. Llm4sgg: Large language model for weakly supervised scene graph generation. In *Proceedings of the IEEE/CVF Conference on Computer Vision and Pattern Recognition*, 2024. 3
- [23] Kibum Kim, Kanghoon Yoon, Jaehyeong Jeon, Yeonjun In, Jinyoung Moon, Donghyun Kim, and Chanyoung Park. Llm4sgg: Large language models for weakly supervised scene graph generation. In *Proceedings of the IEEE/CVF Conference on Computer Vision and Pattern Recognition*, pages 28306–28316, 2024. 3
- [24] Ranjay Krishna, Yuke Zhu, Oliver Groth, Justin Johnson, Kenji Hata, Joshua Kravitz, Stephanie Chen, Yannis Kalantidis, Li-Jia Li, David A Shamma, et al. Visual genome: Connecting language and vision using crowdsourced dense image annotations. *International journal of computer vision*, 123:32–73, 2017. 1, 3
- [25] Sanjoy Kundu and Sathyanarayanan N Aakur. Is-ggt: Iterative scene graph generation with generative transformers. In *Proceedings of the IEEE/CVF Conference on Computer Vision and Pattern Recognition*, pages 6292–6301, 2023. 2, 3, 4
- [26] Linjie Li, Yen-Chun Chen, Yu Cheng, Zhe Gan, Licheng Yu, and Jingjing Liu. Hero: Hierarchical encoder for video+ language omni-representation pre-training. *arXiv preprint arXiv:2005.00200*, 2020. 2
- [27] Rongjie Li, Songyang Zhang, and Xuming He. Sgtr: End-to-end scene graph generation with transformer. In *proceedings of the IEEE/CVF conference on computer vision and pattern recognition*, pages 19486–19496, 2022. 2, 3, 4, 5
- [28] Yuanzhi Liang, Yalong Bai, Wei Zhang, Xueming Qian, Li Zhu, and Tao Mei. Vrr-vg: Refocusing visually-relevant relationships. In *Proceedings of the IEEE/CVF international conference on computer vision*, pages 10403–10412, 2019. 3
- [29] Yao Liu, Lina Yao, Binghao Li, Xianzhi Wang, and Claude Sammut. Social graph transformer networks for pedestrian trajectory prediction in complex social scenarios. In *Proceedings of the 31st ACM International Conference on Information & Knowledge Management*, pages 1339–1349, 2022. 2
- [30] Yanan Liu, Hao Zhang, Dan Xu, and Kangjian He. Graph transformer network with temporal kernel attention for skeleton-based action recognition. *Knowledge-Based Systems*, 240:108146, 2022. 2
- [31] Sayak Nag, Kyle Min, Subarna Tripathi, and Amit K Roy-Chowdhury. Unbiased scene graph generation in videos. In *Proceedings of the IEEE/CVF Conference on Computer Vision and Pattern Recognition*, pages 22803–22813, 2023. 3, 4
- [32] Trong-Thuan Nguyen, Pha Nguyen, and Khoa Luu. Hig: Hierarchical interlacement graph approach to scene graph generation in video understanding. In *Proceedings of the IEEE/CVF Conference on Computer Vision and Pattern Recognition*, 2024. 2, 3, 4, 5, 7, 8
- [33] Trong-Thuan Nguyen, Pha Nguyen, Li Xin, Cothren Jackson, Yilmaz Alper, and Khoa Luu. CYCLO: Cyclic graph transformer approach to multi-object relationship modeling in aerial videos. In *The Thirty-eighth Annual Conference on Neural Information Processing Systems*, 2024. 2, 3, 4, 5, 6, 7, 8
- [34] Anwesha Pal, Yiding Qiu, and Henrik Christensen. Learning hierarchical relationships for object-goal navigation. In *Conference on Robot Learning*, pages 517–528. PMLR, 2021. 2
- [35] Yunsheng Pang, Qiuhong Ke, Hossein Rahmani, James Bailey, and Jun Liu. Igformer: Interaction graph transformer for skeleton-based human interaction recognition. In *European Conference on Computer Vision*, pages 605–622. Springer, 2022. 2
- [36] Xufeng Qian, Yueting Zhuang, Yimeng Li, Shaoning Xiao, Shiliang Pu, and Jun Xiao. Video relation detection with spatio-temporal graph. In *Proceedings of the 27th ACM international conference on multimedia*, pages 84–93, 2019. 3, 4
- [37] Xindi Shang, Donglin Di, Junbin Xiao, Yu Cao, Xun Yang, and Tat-Seng Chua. Annotating objects and relations in user-generated videos. In *Proceedings of the 2019 on International Conference on Multimedia Retrieval*, pages 279–287, 2019. 3
- [38] Xindi Shang, Yicong Li, Junbin Xiao, Wei Ji, and Tat-Seng Chua. Video visual relation detection via iterative inference. In *Proceedings of the 29th ACM international conference on Multimedia*, pages 3654–3663, 2021. 4
- [39] Xindi Shang, Tongwei Ren, Jingfan Guo, Hanwang Zhang, and Tat-Seng Chua. Video visual relation detection. In *Proceedings of the 25th ACM international conference on Multimedia*, pages 1300–1308, 2017. 3
- [40] Yuhua Shen and Ehsan Elhamifar. Progress-aware online action segmentation for egocentric procedural task videos. In *Proceedings of the IEEE/CVF Conference on Computer Vision and Pattern Recognition*, pages 18186–18197, 2024. 2
- [41] Yao Teng, Limin Wang, Zhifeng Li, and Gangshan Wu. Target adaptive context aggregation for video scene graph generation. In *Proceedings of the IEEE/CVF International Conference on Computer Vision*, pages 13688–13697, 2021. 2, 3, 4, 5
- [42] Yao-Hung Hubert Tsai, Santosh Divvala, Louis-Philippe Morency, Ruslan Salakhutdinov, and Ali Farhadi. Video relationship reasoning using gated spatio-temporal energy graph. In *Proceedings of the IEEE/CVF Conference on Computer Vision and Pattern Recognition*, pages 10424–10433, 2019. 4
- [43] Ashish Vaswani, Noam Shazeer, Niki Parmar, Jakob Uszkoreit, Llion Jones, Aidan N Gomez, Łukasz Kaiser, and Illia Polosukhin. Attention is all you need. *Advances in neural information processing systems*, 30, 2017. 2
- [44] Guan Wang, Zhimin Li, Qingchao Chen, and Yang Liu. Oed: Towards one-stage end-to-end dynamic scene graph generation. In *Proceedings of the IEEE/CVF Conference on Computer Vision and Pattern Recognition*, pages 27938–27947, 2024. 2, 4, 5
- [45] Jinghao Wang, Zhengyu Wen, Xiangtai Li, Zujin Guo, Jingkan Yang, and Ziwei Liu. Pair then relation: Pair-net for panoptic scene graph generation. *IEEE Transactions on Pattern Analysis and Machine Intelligence*, 2024. 3
- [46] Tao Wu, Runyu He, Gangshan Wu, and Limin Wang. Sportsshi: A dataset for human-human interaction detection in sports videos. In *Proceedings of the IEEE/CVF Conference on Computer Vision and Pattern Recognition*, 2024. 3
- [47] Junbin Xiao, Angela Yao, Zhiyuan Liu, Yicong Li, Wei Ji, and Tat-Seng Chua. Video as conditional graph hierarchy for multi-granular question answering. In *Proceedings of the AAAI Conference on Artificial Intelligence*, volume 36, pages 2804–2812, 2022. 2
- [48] Junbin Xiao, Pan Zhou, Angela Yao, Yicong Li, Richang Hong, Shuicheng Yan, and Tat-Seng Chua. Contrastive video question answering via video graph transformer. *IEEE Transactions on Pattern Analysis and Machine Intelligence*, 45(11):13265–13280, 2023. 2
- [49] Danfei Xu, Yuke Zhu, Christopher B Choy, and Li Fei-Fei. Scene graph generation by iterative message passing. In *Proceedings of the IEEE conference on computer vision and pattern recognition*, pages 5410–5419, 2017. 1, 3
- [50] Biao Yang, Fucheng Fan, Rongrong Ni, Hai Wang, Ammar Jafaripour-imchahi, and Hongyu Hu. A multi-task learning network with a collision-aware graph transformer for traffic-agents trajectory prediction. *IEEE Transactions on Intelligent Transportation Systems*, 25(7):6677–6690, 2024. 2
- [51] Jingkan Yang, Yi Zhe Ang, Zujin Guo, Kaiyang Zhou, Wayne Zhang, and Ziwei Liu. Panoptic scene graph generation. In *European Conference on Computer Vision*, pages 178–196. Springer, 2022. 1, 3
- [52] Jingkan Yang, Wenxuan Peng, Xiangtai Li, Zujin Guo, Liangyu Chen, Bo Li, Zheng Ma, Kaiyang Zhou, Wayne Zhang, Chen Change Loy, et al. Panoptic video scene graph generation. In *Proceedings of the IEEE/CVF Conference on Computer Vision and Pattern Recognition*, pages 18675–18685, 2023. 2, 3, 4, 8
- [53] Di Yao, Haonan Hu, Lun Du, Gao Cong, Shi Han, and Jingping Bi. Trajgat: A graph-based long-term dependency modeling approach for trajectory similarity computation. In *Proceedings of the 28th ACM*



- SIGKDD conference on knowledge discovery and data mining*, pages 2275–2285, 2022. [2](#)
- [54] Seongjun Yun, Minbyul Jeong, Raehyun Kim, Jaewoo Kang, and Hyunwoo J Kim. Graph transformer networks. *Advances in neural information processing systems*, 32, 2019. [2](#)
- [55] Ce Zhang, Simon Stepputtis, Joseph Campbell, Katia Sycara, and Yaqi Xie. Hiker-sgg: Hierarchical knowledge enhanced robust scene graph generation. In *Proceedings of the IEEE/CVF Conference on Computer Vision and Pattern Recognition*, pages 28233–28243, 2024. [2](#)
- [56] Zhu Zhang, Zhou Zhao, Yang Zhao, Qi Wang, Huasheng Liu, and Lianli Gao. Where does it exist: Spatio-temporal video grounding for multi-form sentences. In *Proceedings of the IEEE/CVF Conference on Computer Vision and Pattern Recognition*, pages 10668–10677, 2020. [3](#)
- [57] Chengyang Zhao, Yikang Shen, Zhenfang Chen, Mingyu Ding, and Chuang Gan. Textpsg: Panoptic scene graph generation from textual descriptions. In *Proceedings of the IEEE/CVF International Conference on Computer Vision*, pages 2839–2850, 2023. [3](#)
- [58] Yifeng Zhu, Jonathan Tremblay, Stan Birchfield, and Yuke Zhu. Hierarchical planning for long-horizon manipulation with geometric and symbolic scene graphs. In *2021 IEEE International Conference on Robotics and Automation (ICRA)*, pages 6541–6548. Ieee, 2021. [2](#)